Nano Today (2014) 9, 550—559

Available online at www.sciencedirect.com

ScienceDirect

journal homepage: www.elsevier.com/locate/nanotoday

RAPID COMMUNICATION

Drug-induced amplification of nanoparticle targeting to tumors

Kevin Y. Lin[a], **Ester J. Kwon**[b], **Justin H. Lo**[c,d], **Sangeeta N. Bhatia**[b,d,e,f,g,*]

[a] *Department of Chemical Engineering, Massachusetts Institute of Technology, Cambridge, MA 02139, USA*
[b] *Harvard-MIT Division of Health Sciences and Technology, Massachusetts Institute of Technology, Cambridge, MA 02139, USA*
[c] *Medical Scientist Training Program, Harvard Medical School, Boston, MA 02115, USA*
[d] *Broad Institute of Harvard and MIT, Cambridge, MA 02142, USA*
[e] *Department of Medicine, Brigham and Women's Hospital, Boston, MA 02115, USA*
[f] *Electrical Engineering and Computer Science, David H. Koch Institute for Integrative Cancer Research, MIT, Cambridge, MA 02139, USA*
[g] *Howard Hughes Medical Institute, Chevy Chase, MD 20815, USA*

Received 13 June 2014; received in revised form 19 August 2014; accepted 1 September 2014
Available online 23 September 2014

KEYWORDS
Nanomedicine;
Active targeting;
Cancer therapy;
Vascular disrupting agent;
Liposomes;
Magnetic nanoworms

Abstract Nanomedicines have the potential to significantly impact cancer therapy by improving drug efficacy and decreasing off-target effects, yet our ability to efficiently home nanoparticles to disease sites remains limited. One frequently overlooked constraint of current active targeting schemes is the relative dearth of targetable antigens within tumors, which restricts the amount of cargo that can be delivered in a tumor-specific manner. To address this limitation, we exploit tumor-specific responses to drugs to construct a cooperative targeting system where a small molecule therapeutic modulates the disease microenvironment to amplify nanoparticle recruitment *in vivo*. We first administer a vascular disrupting agent, ombrabulin, which selectively affects tumors and leads to locally elevated presentation of the stress-related protein, p32. This increase in p32 levels provides more binding sites for circulating p32-targeted nanoparticles, enhancing their delivery of diagnostic or therapeutic cargos to tumors. We show

* Corresponding author at: Massachusetts Institute of Technology, 77 Massachusetts Avenue, Building 76-453, Cambridge, MA 02139, USA. Tel.: +1 617 324 0610.
E-mail addresses: kylin@mit.edu (K.Y. Lin), ekwon@mit.edu (E.J. Kwon), jhlo@mit.edu (J.H. Lo), sbhatia@mit.edu (S.N. Bhatia).

http://dx.doi.org/10.1016/j.nantod.2014.09.001

that this cooperative targeting system recruits over five times higher doses of nanoparticles to tumors and decreases tumor burden when compared with non-cooperative controls. These results suggest that using nanomedicine in conjunction with drugs that enhance the presentation of target antigens in the tumor environment may be an effective strategy for improving the diagnosis and treatment of cancer.

Introduction

Nanotechnology has enabled numerous novel and improved approaches for cancer diagnosis and therapy. In particular, active targeting of nanoparticles, or the attachment of affinity ligands to the surface of particles to recognize and bind pathological markers, has arisen as an attractive strategy to precisely deliver cargos to disease sites while simultaneously reducing side effects [1]. Efforts to improve the targeting of nanomaterials have largely focused on engineering the properties of individual nanoparticles, including geometry, surface chemistry, ligand type, and ligand density [2—4]. However, one major factor that limits the effectiveness of active targeting is the paucity of targetable antigens available for nanoparticle binding within a tumor [5]. A promising approach for overcoming this limitation is to leverage disease responses to therapy to greatly enhance the number of existing binding sites, or induce the presentation of novel targets. Previously, localized treatments such as radiation [6] and hyperthermia [7,8] have been used to induce the expression of vascular antigens that serve as binding targets to recruit nanoparticles to tumors. Unfortunately, application of these methods is confined to clinical scenarios where disease sites are known and accessible, and thus preclude the treatment of disseminated disease, which is the primary cause of mortality in cancer [9].

Our strategy is to identify proteins that are selectively induced in the tumor microenvironment following treatment with drugs and leverage them as receptors for targeted nanoparticles. The arsenal of systemic therapies designed to treat metastatic cancer includes traditional cytotoxic drugs [10], molecularly targeted agents [11,12], immunotherapy [13,14], and vascular disrupting agents (VDAs) [15,16], which operate through distinct modes of action. These drugs are attractive inducing agents because many are clinically-approved or in trial stages and are frequently administered in combination with other therapeutics [11,12,17]. Drug-induced antigens have been utilized as biomarkers of therapeutic responses or as antibody targets [18—20], but to our knowledge, these changes have never been used to target nanoparticles to tumors. Here, we investigate the ability of systemically administered drugs to increase the prevalence of tumor-specific antigens to amplify nanoparticle targeting to tumors. In this report, we demonstrate that the small molecule VDA, ombrabulin, enhances the presentation of a stress protein called p32 in human tumor xenografts implanted in mice (Figure 1). p32 is specifically expressed in tumors and serves as the target receptor of the cyclic nonapeptide, LyP1, which was discovered through *in vivo* phage display [21,22]. We then use ombrabulin to induce greater levels of p32 in tumors and deliver two different LyP1-decorated nanoparticles to tumors: a prototypical imaging agent (magnetofluorescent iron oxide nanoworms) and a prototypical therapeutic agent (doxorubicin-loaded liposomes). We show that this cooperative targeting system amplifies the recruitment of targeted nanoparticles to tumors by three- to five-fold over non-cooperative controls, and improves the tumor burden and survival of mice in a preclinical therapeutic study.

Results

Characterization of ombrabulin-induced p32 presentation

Ombrabulin is a microtubule-binding agent that impacts tumor vasculature by effecting a rapid sequence of events shortly after administration, including morphological and functional changes in endothelial cells that increase vascular permeability, and culminate in extensive hemorrhagic necrosis within the tumor [15,23,24] (Figure 2A and B). Widespread extravasation of red blood cells into the tumor interstitium was observed within 1 h, and central necrosis was evident between 6 and 24 h following drug administration (Figure 2C). The selective vulnerability of tumor vessels to tubulin-binding compounds has been attributed to their immature development and defective pericyte coverage relative to normal vessels [15,16]. We hypothesized that the antitumor activity of ombrabulin might increase tumor presentation of p32 [p33/gC1q receptor/hyaluronan binding protein 1 (HABP1)], a mitochondrial protein that is found at elevated levels on the surface of stressed tumor and tumor-associated cells in a wide range of tumor types, particularly in hypoxic or nutrient-deprived regions [22]. To investigate the ability of ombrabulin to increase p32 presentation within tumors, we intravenously injected different doses of the drug (0, 30, 60 mg/kg) into nude mice ($n = 3$ mice per condition) bearing bilateral human MDA-MB-435 tumors. At 4 and 24 h, mice were euthanized and p32 presentation was assessed *via* immunofluorescent staining of tumor sections (Figure 2D). We observed that the percentage of p32-positive staining within the tumor trended upward with both time and ombrabulin dose, showing nearly a four-fold increase in p32-positive area at 24 h after a 60 mg/kg dose (Figure 2E). To assay for increased p32 presentation at the surface of surviving cancer cells, tumors were dissociated into single cell suspensions for quantification of p32 surface expression by live-cell staining and flow cytometry (Figure S1). Consistent with the trend observed in tumor sections, flow-based examination of the tumor population revealed that the percentage of cancer cells positive for surface p32 increased significantly by up to four-fold at 24 hrs after ombrabulin treatment ($^{***}P < 0.005$ by one-way ANOVA with

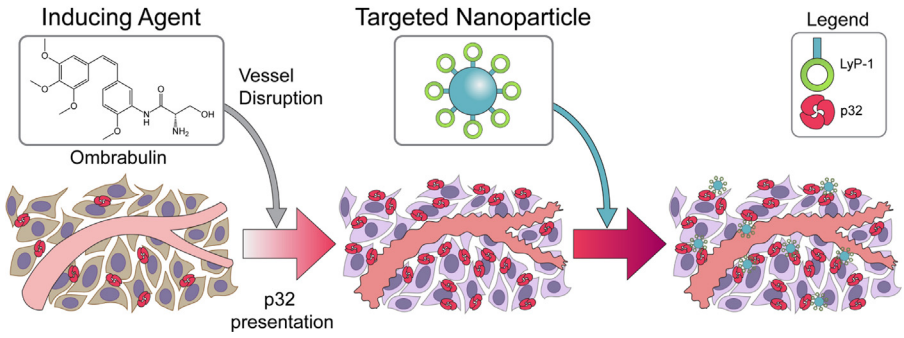

Figure 1 Schematic of cooperative targeting approach. Inducing agent, ombrabulin, disrupts the tumor vasculature, which initiates a cascade of intratumoral effects that lead to upregulated presentation of the p32 protein. LyP-1 coated nanoparticles, which target the p32 protein, are then able to home to the tumor.

Tukey post test; Figure 2F). Together, these data show that exposure to ombrabulin modulates the tumor environment to amplify p32 presentation within the tumor, particularly on the surface of surviving cancer cells.

Ombrabulin-induced amplification of tumor targeting

We next investigated the ability of magnetofluorescent iron oxide nanoworm (NW) imaging agents, a nanoparticle previously developed by our collaborators [25,26], to target tumors following ombrabulin treatment (Figure 3A). The NWs were first derivatized with a near-infrared fluorophore (VT750) to enable detection of their distribution by fluorescence imaging. Then, the NWs were further modified by the attachment *via* PEG of either the cyclic nonapeptide LyP-1 (CGNKRTRGC), which binds p32 and facilitates tissue penetration, or ARAL (ARALPSQRSR), an untargeted peptide that has the same net charge as LyP-1 to control for nonspecific electrostatic interactions of the nanoparticles [7,22,27,28]. The LyP-1 (NW-LyP1) and ARAL (NW-ARAL) conjugated NWs were prepared with similar size distributions and peptide valencies (~40 peptides per NW by absorbance spectroscopy; Figure S2). Additionally, as expected, the NW-LyP1 showed significantly greater binding to purified recombinant p32 *in vitro* relative to NW-ARAL, which validated the selection of ARAL as a non-targeted control sequence (Figure S3A).

To test for amplification of NW targeting to tumors, different doses of ombrabulin (0, 30, 60 mg/kg) were intravenously injected into mice ($n = 3$—4 mice per condition) bearing bilateral MDA-MB-435 tumors, followed by either NW-LyP1 or NW-ARAL administration after 24 h (Figure 3B). At 24 h post-NW injection, *ex vivo* fluorescent imaging of tumors revealed a dose-dependent increase in NW-LyP1 accumulation of up to three-fold relative to no drug controls and without altering the organ distribution of the nanoparticles (Figure 3C and D, Figure S4). The non-targeted NW-ARAL also exhibited a marginal dose-dependent increase in accumulation, which is consistent with previous reports demonstrating the enhanced extravasation of macromolecules following vascular disruption by small molecule therapeutics [29]. Notably, the NW-LyP1 exhibited a significantly greater increase in accumulation of ~1.5—2 fold compared to the NW-ARAL when following ombrabulin treatment ($^{**}P < 0.01$ by Student's *t*-test), which suggested that induction of p32 presentation by ombrabulin leads to amplified targeting of NWs to tumors. Histological examination of tumor sections revealed that the presence of both NW-LyP1 (green) and p32 (red) increased, and localized within ombrabulin-treated tumors (60 mg/kg) *versus* untreated tumors, while NW-ARAL (green) staining was less intense and did not colocalize with p32 (red) in either scenario (Figure 3E). We also explored an alternative dosing sequence in which ombrabulin and NWs were injected simultaneously and found that co-administration did not lead to a pronounced difference in accumulation between NW-LyP1 and NW-ARAL (Figure S5). This result is consistent with the previous finding that enhancement of p32 presentation takes up to 24 h post-ombrabulin treatment, and supports the hypothesis that p32 binding is necessary for the enhanced targeting of NW-LyP1. Collectively, these data show that pre-exposure to ombrabulin mediates the amplification of NW homing to tumors by increasing the amount of the target p32 protein available for binding.

Ombrabulin-induced amplification of therapeutic delivery

We next constructed model therapeutic nanoparticles, doxorubicin-loaded liposomes (LP), to test for amplified drug delivery to regions of ombrabulin-induced p32 presentation in tumors (Figure 4A). LPs were synthesized with either the targeting peptide LyP1 (LP-LyP1) or the control peptide ARAL (LP-ARAL) on the surface of particles and both populations were confirmed to exhibit similar size distributions (Figure S6) [7]. To test for amplification of LP targeting to tumors, mice ($n = 3$ mice per condition) bearing bilateral MDA-MB-435 tumors were intravenously injected with either saline or ombrabulin (60 mg/kg), followed by LP-LyP1 or LP-ARAL (1 mg/kg by dox) after 24 h. At 24 h post-LP injection, we found that ombrabulin treatment amplified the delivery of LP-LyP1 and accumulation of doxorubicin in tumors by ~four-fold *versus* non-targeted LP-ARAL, ~2.5 fold relative to LP-LyP1 alone, and ~five-fold relative to non-cooperative and non-targeted LP-ARAL ($^{***}P < 0.005$ by Student's *t*-test; Figure 4B). Notably, without ombrabulin, LP-LyP1 also demonstrated higher accumulation

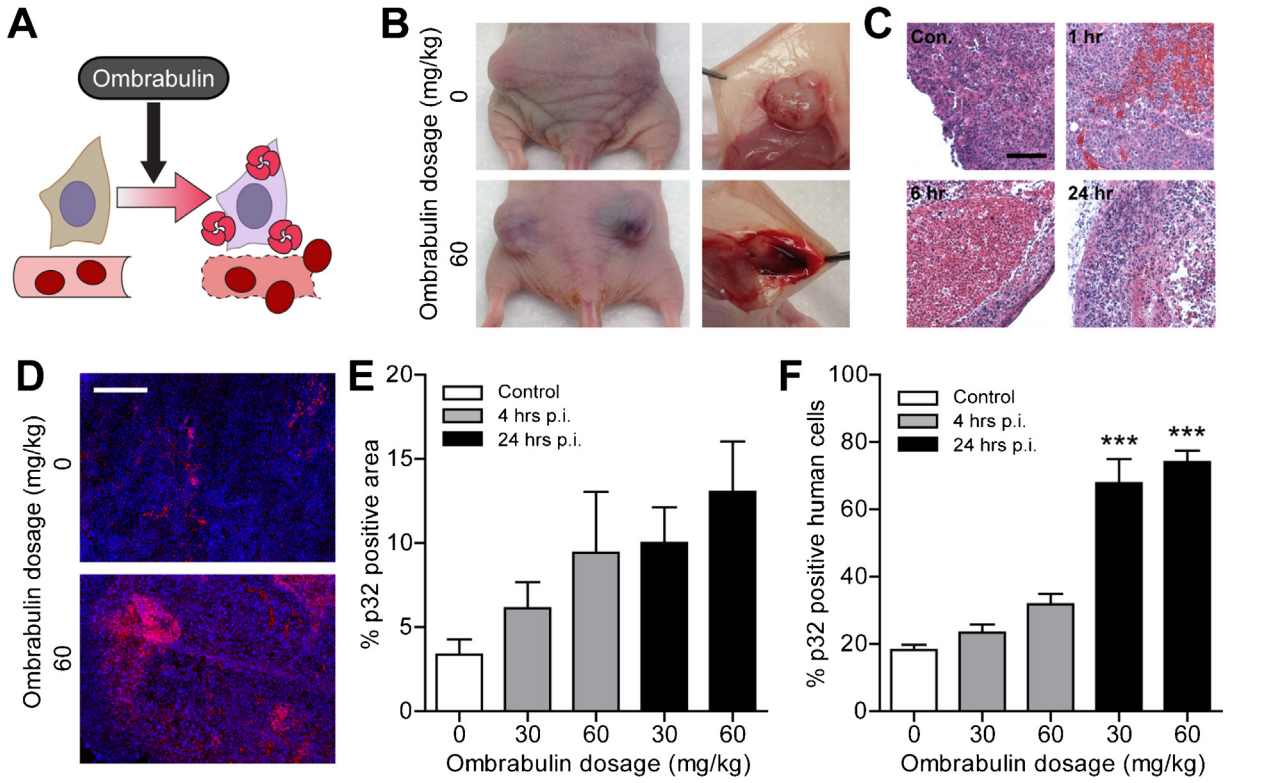

Figure 2 Characterization of ombrabulin effect on tumor microenvironment. (A) Schematic of ombrabulin-induced enhancement in p32 presentation. (B) Tumors at 24 h post injection (p.i.) revealing ombrabulin mediated hemorrhaging. (C) Hematoxylin and eosin staining of tumors harvested from mice injected with ombrabulin at different timepoints p.i. (Con., control (0 mg/kg); scale bar = 100 μm). (D) Immunofluorescent staining of tumors without (0 mg/kg) and with (60 mg/kg) ombrabulin (red = p32 staining, blue = nuclear stain; scale bar = 1 mm). (E) Quantification of percentage p32 positive area of immunofluorescent staining of tumors receiving different dosages of ombrabulin at different timepoints p.i. ($n = 3$ mice, s.e.). (F) Quantification of percentage p32 positive human cells from tumors receiving different dosages of ombrabulin at different timepoints as determined by flow cytometry ($^{***}P < 0.005$, one-way ANOVA with Tukey post test; $n = 3$ mice, s.e.). (For interpretation of the references to color in this figure legend, the reader is referred to the web version of this article.)

of doxorubicin in tumors than LP-ARAL, which was consistent with previous studies using nanoparticles targeted by LyP1 [30—32]. Similar to the NWs, histological examination of tumor sections again showed increased, localized staining of both LP-LyP1 (green) and p32 (red) in ombrabulin-treated tumors *versus* untreated tumors, while LP-ARAL (green) staining was sparsely distributed and did not localize to areas with p32 (red) in either scenario (Figure 4C). We also investigated the organ distribution of doxorubicin following cooperative targeting and found that administration of both ombrabulin and LP-LyP1 or LP-ARAL did not change the biodistribution of doxorubicin, with a majority of the drug accumulating in the spleen and liver (Figure 4D). This result indicated that despite being administered systemically, ombrabulin does not lead to the increased accumulation of LPs in off-target sites and that the majority of particles are still cleared by the organs associated with the reticuloendothelial system, which is typical of systemically administered nanomaterials [4]. Altogether, these experiments showed that pre-treatment with ombrabulin amplified the delivery of therapeutic nanoparticles that target the p32 protein.

Amplified tumor therapy with cooperative therapeutics

Finally, we evaluated the therapeutic efficacy of cooperative targeting in mice ($n = 7$ mice per condition) bearing single MDA-MB-435 human carcinoma tumors. Ombrabulin (60 mg/kg) or saline were injected into mice and 24 h later, an intravenous dose of LP-LyP1, LP-ARAL (2 mg/kg by dox), or saline was given. When this treatment regimen was administered every 4—5 days, we found that ombrabulin + LP-LyP1 was significantly more effective at slowing tumor growth ($^{*}P < 0.05$ by two-way ANOVA with Bonferroni post test) than the treatments in isolation (ombrabulin, LP-LyP1, LP-ARAL) and non-cooperative controls (ombrabulin + LP-ARAL; Figure 5A, Figure S7) without any significant changes in animal weight following the last cycle of treatment (Figure 5B). In comparing the long term survival of mice in the various treatment groups, we found that ombrabulin + LP-LyP1 significantly prolonged the survival time of mice relative to all other treatments ($^{**}P < 0.01$ by log rank test, $n = 7$ mice; Figure 5C). Collectively, these therapeutic studies demonstrated that the cooperativity of

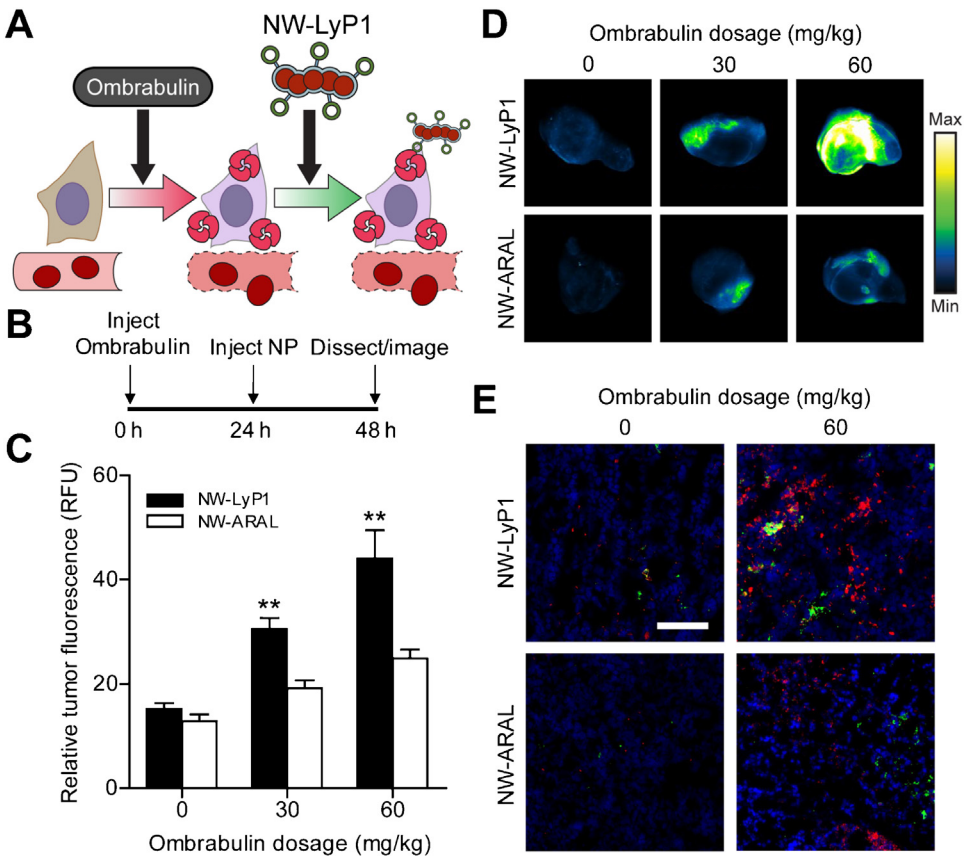

Figure 3 Ombrabulin mediated amplification of NW delivery. (A) Schematic of ombrabulin signaling to NWs. Ombrabulin upregulates the presentation of p32 in tumors, which is then targeted by NW-LyP1. (B) Experimental timeline for testing the signaling system. (C) Quantification of NW homing to tumors as a function of ombrabulin dosage (** $P < 0.01$, Student's t-test; $n = 3$—4 mice, s.e.). (D) Representative near-infrared fluorescent scans of NW homing to tumors in response to increasing doses of ombrabulin. Tumors were excised and imaged at 24 h post-NW injection. (E) Immunofluorescent staining of NWs in tumors without (0 mg/kg) and with (60 mg/kg) ombrabulin (green = NW, red = p32 staining, blue = nuclear stain; scale bar = 100 μm). (For interpretation of the references to color in this figure legend, the reader is referred to the web version of this article.)

ombrabulin and targeted LPs led to decreased tumor growth and prolonged survival of mice.

Discussion

In this study, we design a cooperative targeting system that harnesses the ombrabulin-induced increase in presentation of p32 to amplify the recruitment of two model nanoparticle systems which are actively targeted to tumors. Using small molecules or proteins to modulate the disease environment is advantageous because they do not face the same extravasation and diffusion barriers as larger vehicles [33], and may therefore effectively prime the tumor microenvironment for subsequent nanoparticle delivery. Numerous related strategies have aimed to enhance nanoparticle accumulation by increasing vascular permeability through the administration of vasoactive agents such as vascular endothelial growth factor, bradykinin, and tumor necrosis factor alpha [34]. However, a general concern with these approaches is that they may affect both healthy and diseased vasculature, thus escalating the risk of off-target effects. In contrast, our method leverages the specificity of ombrabulin for tumor vasculature, which is derived from the increased susceptibility of immature vessels to tubulin-binding agents [15,16], and the tumor-specific expression of cell-surface p32 to bolster nanoparticle accumulation while simultaneously minimizing off-target delivery [22]. Compared to an earlier study performed by our group using gold nanorod-mediated hyperthermia, administration of ombrabulin produced a larger increase in the magnitude of tumor p32 expression and a similar fold enhancement in nanoparticle homing to tumors [7]. However, this system offers several advantages over the previously described cooperative system that may impact translation into the clinical setting. First, gold nanorods used in the previous system must overcome significant size-dependent diffusion barriers compared to small molecule VDAs in order to penetrate deep into tumors, actuate the p32 signal throughout the disease site, and facilitate amplified delivery of the second cargo [35]. Additionally, gold nanorod-mediated hyperthermia requires exposing the nanorods to a near-infrared laser, which has a limited penetration depth through tissue, thereby precluding the treatment of tumors located deep within the body [36]. Finally, unlike previous systems that utilize localized and guided treatment modalities such as hyperthermia [7,8] and radiation therapy [6] to induce the presentation of

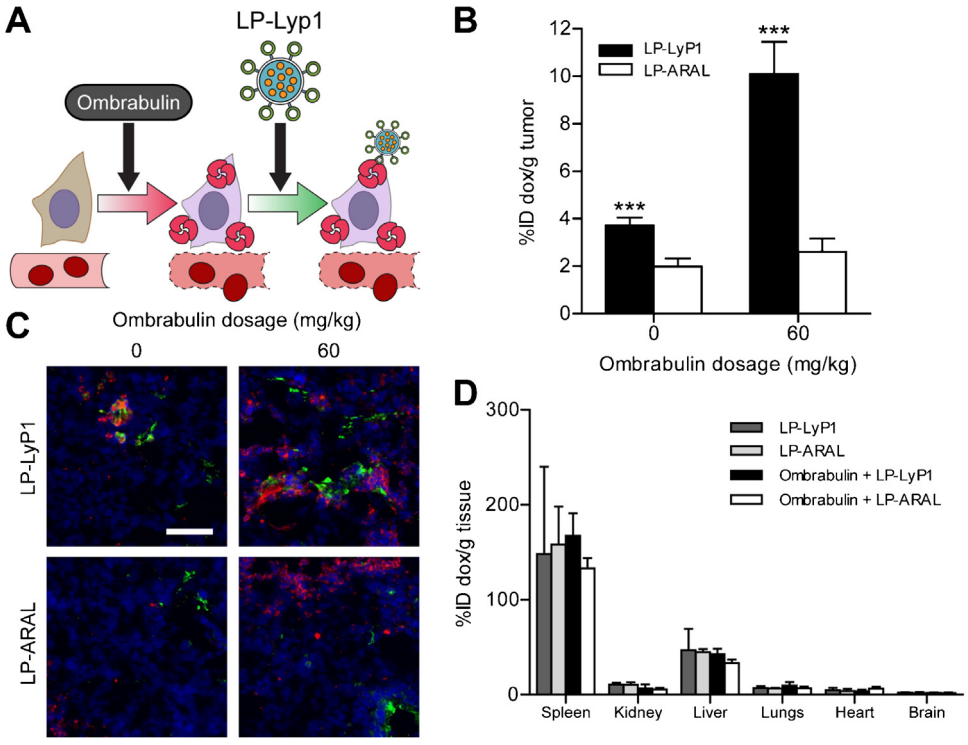

Figure 4 Ombrabulin mediated amplification of LP delivery. (A) Schematic of ombrabulin signaling to LPs. Ombrabulin upregulates the presentation of p32 in tumors, which is then targeted by LP-LyP1. (B) Quantification of doxorubicin-loaded LP homing to tumors as a function of ombrabulin dosage (*** $P < 0.005$, Student's t-test; $n = 3$ mice, s.e.). (C) Immunofluorescent staining of LPs in tumors without (0 mg/kg) and with (60 mg/kg) ombrabulin (green = LP, red = p32 staining, blue = nuclear stain; scale bar = 100 μm). (D) Quantification of doxorubicin-loaded LP biodistribution in organs without (0 mg/kg) and with (60 mg/kg) ombrabulin (no significance, one-way ANOVA with Tukey post test; $n = 3$—6 mice, s.d.). For interpretation of the references to color in this figure legend, the reader is referred to the web version of this article.)

novel binding sites, our strategy is fully autonomous with the potential to survey the entire body for disseminated disease without any *a priori* knowledge of tumor locations.

Vascular disrupting agents like ombrabulin are attractive inducing agents to be used in this cooperative targeting system not only because of their anti-vascular activity against a broad range of tumor types [23,37], but because preclinical and clinical studies suggest that VDAs have the greatest impact when coupled with other treatments; as single agents, VDAs leave a viable tumor rim that can obtain nutrients and oxygen from neighboring healthy tissues and rapidly re-grow [15,16,24]. Here, we demonstrated that pre-treatment of tumors with ombrabulin amplified the delivery of both prototypical diagnostic and therapeutic nanoparticles, highlighting the modularity of this stigmergic targeting approach. This data suggests that this system may be applicable to any number of cargos that are deliverable by nanoparticles, including other chemotherapies, siRNA, or diagnostic markers [1,2,38]. Vascular disrupting agents and traditional chemotherapy have previously been coupled together in a single nanoparticle formulation and shown to be therapeutically effective, but these efforts did not incorporate any form of active targeting [39]. Our therapeutic study showed that cooperative targeting was not only more effective than either agent alone, but also was advantageous compared to the combination of ombrabulin and control non-targeted liposomes. These results also suggest that the staggered administration of a cooperative combination of drug and targeted nanoparticle may generate positive therapeutic indices by enhancing the delivery of cargos. Furthermore, recent studies have highlighted the importance of optimizing the dosing schedule for combination therapies involving VDAs given their range of temporal effects, with most recent results supporting the pretreatment of tumors with VDA prior to chemotherapy [40,41]. The protocol and results of our cooperative strategy were consistent with these findings, showing a greater enhancement in nanoparticle accumulation when they were administered 24 h after ombrabulin *versus* when they were co-administered.

Looking forward, several experimental avenues warrant further investigation in order to expand the applicability of cooperative nanoparticle targeting. In this study, we used a VDA to increase the number of nanoparticle binding sites within tumors, however the current arsenal of cancer treatments includes many other candidates with the potential to serve as inducing agents for cooperative targeting approaches. In addition to the aforementioned treatment modalities, traditional chemotherapies and next-generation targeted therapies have also been used to induce tumor antigens, which were identified by either gene expression profiling [20,42] or *in vivo* phage display [18,19]. Future studies may focus on developing systematic screening approaches to identify novel induced antigens in response to panels of drugs spanning multiple classes. These

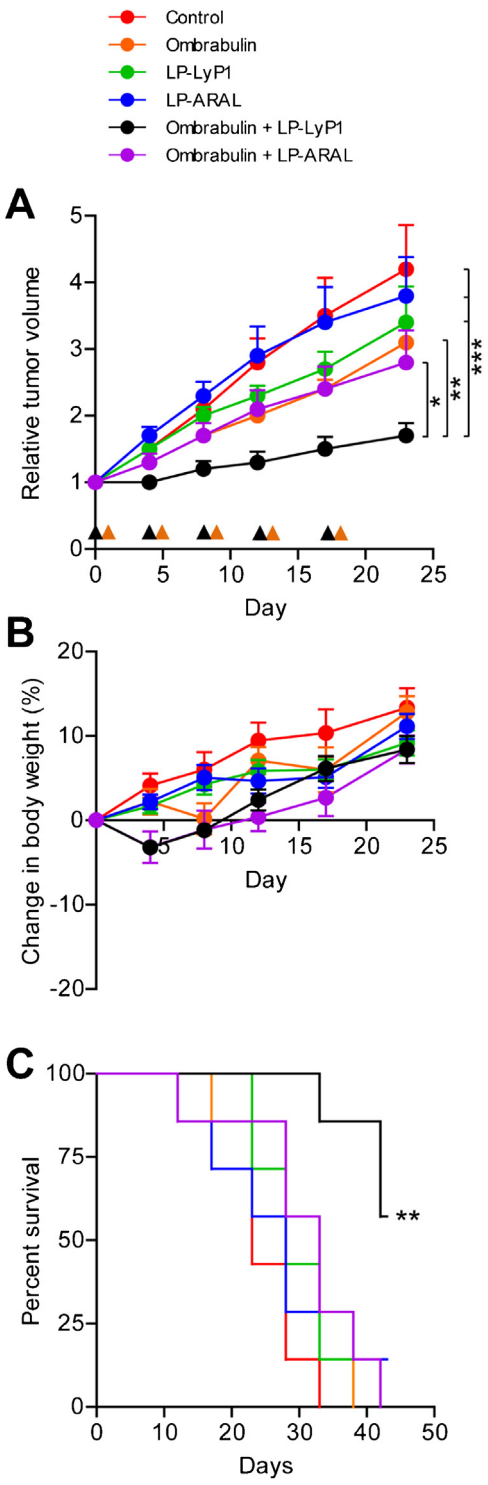

Figure 5 Therapeutic efficacy of cooperative targeting system. (A) Tumor volumes of different groups following three weeks of treatment. Black arrow head denotes time of ombrabulin (60 mg/kg) administration; orange arrow head denotes time of LP (1 mg/kg by dox) administration (* $P < 0.05$, ** $P < 0.01$, *** $P < 0.005$, two-way ANOVA with Bonferroni post test, $n = 7$ mice, s.e.). (B) Change in body weight of different groups following three weeks of treatment ($n = 7$ mice, s.e.). (C) Survival rate of different groups in the therapeutic efficacy study (** $P < 0.01$, log rank test; $n = 7$ mice).

antigens could then be cross-referenced to known libraries of targeting ligands from the literature or used to develop new ligands in order to create more potential pairings of cooperative drugs and ligand-decorated nanoparticles. In summary, this work introduces a new approach for designing nanoparticle targeting systems that leverages drug-induced modulation of the disease environment to improve the detection and treatment of cancer.

Materials and methods

Generation of MDA-MB-435 xenografts

MDA-MB-435 cancer cell lines (American Type Culture Collection) were cultured in Dulbecco's Modified Eagle Medium (DMEM) with 10% fetal bovine serum, penicillin, and streptomycin. To generate subcutaneous xenograft models, 4–6-week-old female NCr nude mice (Taconic) were injected either laterally or bilaterally in the hind flanks, according to the experimental design, with $\sim 2 \times 10^6$ MDA-MB-435 cells suspended in 200 μL DMEM.

Histological analysis

Ombrabulin was kindly provided by Sanofi Aventis. Mice bearing bilaterial flank MDA-MB-435 xenografts ($n = 3$ mice) were intravenously administered different dosages of ombrabulin (0, 30, 60 mg/kg) in 0.9% NaCl without anesthesia. At different time points (4, 24 h p.i.) the mice were euthanized and their tumors were excised. For hematoxylin and eosin staining, tumors were fixed in 4% paraformaldehyde for 1–2 h at RT and stored in 70% ethanol until paraffin-embedding, sectioning, and staining (Koch Institute Histology Core). For immunofluorescent staining, representative frozen tumor sections were stained for p32 (Millipore) and Hoechst (Invitrogen) before analysis by fluorescence microscopy (Nikon Eclipse Ti). The percentage of p32 positive staining in the tumor was quantified using MATLAB (MathWorks).

Flow cytometry

Ombrabulin (0, 30, or 60 mg/kg) was administered intravenously to mice bearing bilateral flank MDA-MB-435 xenografts. At different time points (4 or 24 h post-injection), the mice were euthanized and their tumors were excised in their entirety. The tumors were gently dissociated into single cell suspensions using a MACS human Tumor Dissociation Kit (Miltenyi Biotec) according to manufacturer instructions. 2.5×10^6 cells per condition were incubated for 1 h on ice with both Alexa Fluor-488-conjugated mouse anti-human HLA-AB (BD Pharmingen) and either rabbit polyclonal anti-p32 (Millipore) or rabbit IgG isotype control (R&D Systems). Cells were then washed twice with cold PBS supplemented with 2% fetal bovine serum (FBS), followed by incubation for 1 h on ice with Alexa Fluor-594 goat anti-rabbit secondary antibody (Invitrogen). Cells were washed and then resuspended in PBS plus 2% FBS for analysis. For quantification of surface p32 levels, human tumor cells were isolated by gating out all HLA-ABC-negative cells.

Peptide nanoworm synthesis

Aminated iron oxide NWs were synthesized according to previously published protocols [26]. Peptides (LyP1 = C-(K-Flsc)-C6-CGNKRTRGC, Cys2 & Cys3 bridge; ARAL = C-(K-Flsc)-C6-ARALPSQRSR; Flsc = fluorescein, C6 = 6-aminohexanoic acid linker) were synthesized by CPC Scientific and the Tufts University Core Facility peptide synthesis service. To conjugate peptides to NWs, NWs were first reacted with NHS-VivoTag 750 (VT750, PerkinElmer) and MAL-PEG(5k)-SVA (Laysan Bio.) to introduce sulfhydryl-reactive handles. Cysteine terminated peptides were then mixed with NWs (95:1 molar ratio) for 1 h at room temperature (RT) and purified using a Sephadex G-25 gel filtration column (GE Healthcare). Stock solutions were stored in PBS at 4 °C. The number of fluorescein-labeled peptides per NWs was determined by absorbance spectroscopy using the absorbance of fluorescein (490 nm) and its extinction coefficient (78,000 $cm^{-1} M^{-1}$). The particle size was measured by dynamic light scattering (Malverin Zetasizer Nano Series).

Doxorubicin-loaded liposome synthesis

Hydrogenated soy sn-glycero-3-phosphocholine (HSPC), cholesterol, and 1,2-distearoyl-snglycero-3-phosphoethanolamine-N-polyethylene glycol 2000 [DSPE-PEG(2k)] were purchased from Avanti Polar Lipids. DSPE-[Maleimide(Polyethylene Glycol 5000)] [DSPE-PEG(5K)-MAL was purchase from Nanocs, Inc. Doxorubicin was purchased from Sigma Chemical Co. For peptide conjugation, DSPE-PEG(5K)-MAL was reacted with Cysteine-terminated peptides (LyP1 or ARAL) in 50 mM triethylamine, DMF for 24 h and exchanged into water using gel filtration. Liposomes were prepared from HSPC, cholesterol, and either DSPE-PEG(5K)-LyP1 or DSPE-PEG(5K)-ARAL in the molar ratio of 75:50:3 by the lipid film hydration and membrane (100 nm) extrusion method [43]. Encapsulation of doxorubicin (dox) into the liposomes was then carried out using the pH gradient-driven loading protocol [44]. Free doxorubicin was removed by gel filtration on Sephadex G-25. The peptide-conjugated doxorubicin liposomes were stored in PBS at 4 °C before use. The particle size was measured by dynamic light scattering (Malverin Zetasizer Nano Series) and the fluorescence intensity was measured by a microplate reader (SpectroMax Gemini EM, Molecular Devices).

In vitro binding assay

The *in vitro* binding of nanoparticles to p32 was assessed using a magnetic bead assay. Briefly, NWs (40 pmol by Flsc) or LPs (1.5 pmol by Flsc) were incubated with Ni-NTA magnetic agarose beads (Qiagen) coated with His-tagged recombinant p32 protein (kindly provided by Dr. T. Teesalu) in binding and washing buffer (BWB; PBS with 300 mM NaCl, 5 mM imidazole, 0.05% NP-40, 0.1% bovine serum albumin) for 1 h at room temperature, washed four times with BWB, and eluted with 400 mM imidazole in BWB. Samples were quantified with a fluorescence microplate reader (SpectroMax Gemini EM, Molecular Devices) at excitation/emission wavelengths of 485/538 nm and compared to standard curves.

Nanoworm homing to tumors

Mice bearing bilateral flank MDA-MB-435 xenografts ($n = 3$—4 mice) were intravenously administered different dosages of ombrabulin (0, 30, 60 mg/kg). NW-LyP1 or NW-ARAL (1 nmol by VT750) were either co-administered or injected 24 h following ombrabulin administration. At 24 h post-NW administration, organs were removed and scanned on the LI-COR Odyssey Infrared Imaging System. Fluorescence in each organ was quantified using ImageJ software (NIH). To analyze tumors by immunostaining, representative sections were stained for NWs (anti-Flsc primary, GeneTex), either p32 (Millipore) or CD31 (BD Pharmingen), and Hoechst (Invitrogen) before analysis by fluorescence microscopy (Nikon Eclipse Ti).

Quantification of doxorubicin in tissues

Mice bearing bilateral flank MDA-MB-435 xenografts ($n = 3$ mice) were intravenously administered different dosages of ombrabulin (0, 60 mg/kg), followed by either LP-LyP1 or LP-ARAL (1 mg/kg by dox) 24 h later. At 24 h post-LP administration, organs were removed, weighed, incubated with 500 μl of 70% EtOH, 0.3 N HCl, and homogenized (Tissue Tearor, Biospec Products) to release doxorubicin from tissues. Following homogenization, another 1 ml of 70% EtOH, 0.3 N HCl, was added to samples and they were centrifuged. Supernatants of samples were analyzed for doxorubicin fluorescence using a fluorescence microplate reader (SpectroMax Gemini EM, Molecular Devices) at excitation/emission wavelengths of 470/590 nm and compared to standard curves. To analyze tumors by immunostaining, representative sections were stained for LPs (anti-Flsc primary, GeneTex), p32 (Millipore), and Hoechst (Invitrogen) before analysis by fluorescence microscopy (Nikon Eclipse Ti).

Therapeutic assessment of cooperative targeting systems

Treatment of mice commenced 14 days after subcutaneous injection of MDA-MB-435 cancer cells. Tumor dimensions were measured with calipers and the volume was calculated using the modified ellipsoid formula (volume = $1/2 \times \text{length} \times \text{width}^2$), where L and W refer to the larger and smaller perpendicular dimensions collected at each measurement [45]. Mice bearing single lateral xenografts were randomized into groups of seven mice such that the mean tumor volumes were similar between groups. Mice were first administered different dosages of ombrabulin (0, 60 mg/kg). At 24 h post-injection, mice were administered LP-LyP1 (2 mg/kg), LP-ARAL (2 mg/kg), or saline. This treatment regimen was repeated every 4—5 days. At regular intervals after treatment, tumors were measured and mice were weighed. For the survival curve study, mice were sacrificed when tumors exceeded the humane endpoint set at 500 mm^3. To compute the volumetric doubling time of tumors, each tumor volume trace was fit to an exponential growth curve in Excel (Microsoft) and

the doubling time was calculated from the growth constant [46].

Statistical analyses

Student's *t*-test, one- and two-way ANOVA, and survival curve analyses were calculated with GraphPad 5.0 (Prism).

All experimental protocols involving animals were approved by the MIT Committee on Animal Care (protocol #0411-036-14).

Acknowledgments

We thank Joerg Adamczewski, Hichem Chakroun, Patricia Vrignaud, and Chantal Carrez from Sanofi-Aventis for generously providing us with ombrabulin and experimental guidance. We thank Dr. Tambet Teesalu for providing us with recombinant p32. We thank the Koch Institute Swanson Biotechnology Center (MIT) for assistance with tissue sectioning, specifically Michael Brown and Kathleen Cormier from the Histology core. We thank Dr. Heather Fleming (MIT) for critical readings of the manuscript. This work was supported by the NIH (BRP: R01CA124427-01), NIH/NCI (U54CA119349, U54CA119335, and the Alliance Challenge Project/MIT-Harvard Center of Cancer Nanotechnology Excellence: U53CA151884), Packard Fellowship (1999-1453), and Marie-D. & Pierre Casimir-Lambert Fund. This work was supported in part by the Koch Institute Support (core) Grant P30-CA14051 from the National Cancer Institute. K.Y.L. acknowledges support from CCNE (5 U54 CA151884-03). J.H.L. acknowledges support from NIH MSTP program (T32GM007753). Dr. E.J.K. acknowledges support from the Ruth L. Kirschstein National Research Service Award (1F32CA177094-01). Dr. S.N.B is an HHMI Investigator.

Appendix A. Supplementary data

Supplementary data associated with this article can be found, in the online version, at http://dx.doi.org/10.1016/j.nantod.2014.09.001.

References

[1] M. Ferrari, Nat. Rev. Cancer 5 (2005) 161—171.
[2] R.A. Petros, J.M. DeSimone, Nat. Rev. Drug Discov. 9 (2010) 615—627.
[3] J.D. Byrne, T. Betancourt, L. Brannon-Peppas, Adv. Drug. Deliv. Rev. 60 (2008) 1615—1626.
[4] S.-D. Li, L. Huang, Mol. Pharm. 5 (2008) 496—504.
[5] E. Ruoslahti, S.N. Bhatia, M.J. Sailor, J. Cell Biol. 188 (2010) 759—768.
[6] D. Hallahan, L. Geng, S. Qu, C. Scarfone, T. Giorgio, E. Donnelly, X. Gao, J. Clanton, Cancer Cell 3 (2003) 63—74.
[7] J.-H. Park, G. von Maltzahn, M.J. Xu, V. Fogal, V.R. Kotamraju, E. Ruoslahti, S.N. Bhatia, M.J. Sailor, Proc. Natl. Acad. Sci. USA 107 (2010) 981—986.
[8] G. von Maltzahn, J.-H. Park, K.Y. Lin, N. Singh, C. Schwöppe, R. Mesters, W.E. Berdel, E. Ruoslahti, M.J. Sailor, S.N. Bhatia, Nat. Mater. 10 (2011) 545—552.
[9] A.F. Chambers, A.C. Groom, I.C. MacDonald, Nat. Rev. Cancer 2 (2002) 563—572.
[10] B.A. Chabner, T.G. Roberts Jr., Nat. Rev. Cancer 5 (2005) 65—72.
[11] S. Kummar, H.X. Chen, J. Wright, S. Holbeck, M.D. Millin, J. Tomaszewski, J. Zweibel, J. Collins, J.H. Doroshow, Nat. Rev. Drug Discov. 9 (2010) 843—856.
[12] B. Al-Lazikani, U. Banerji, P. Workman, Nat. Biotechnol. 30 (2012) 679—692.
[13] L.M. Weiner, R. Surana, S. Wang, Nat. Rev. Immunol. 10 (2010) 317—327.
[14] I. Mellman, G. Coukos, G. Dranoff, Nature 480 (2011) 480—489.
[15] G.M. Tozer, C. Kanthou, B.C. Baguley, Nat. Rev. Cancer 5 (2005) 423—435.
[16] V.L. Heath, R. Bicknell, Nat. Rev. Clin. Oncol. 6 (2009) 395—404.
[17] V.T. DeVita Jr., R.C. Young, G.P. Canellos, Cancer 35 (1975) 98—110.
[18] Z. Han, A. Fu, H. Wang, R. Diaz, L. Geng, H. Onishko, D.E. Hallahan, Nat. Med. 14 (2008) 343—349.
[19] R.J. Passarella, L. Zhou, J.G. Phillips, H. Wu, D.E. Hallahan, R. Diaz, Clin. Cancer Res. 15 (2009) 6421—6429.
[20] B. Rubinfeld, A. Upadhyay, S.L. Clark, S.E. Fong, V. Smith, H. Koeppen, S. Ross, P. Polakis, Nat. Biotechnol. 24 (2006) 205—209.
[21] P. Laakkonen, K. Porkka, J.A. Hoffman, E. Ruoslahti, Nat. Med. 8 (2002) 751—755.
[22] V. Fogal, L. Zhang, S. Krajewski, E. Ruoslahti, Cancer Res. 68 (2008) 7210—7218.
[23] Y. Morinaga, Y. Suga, S. Ehara, K. Harada, Y. Nihei, M. Suzuki, Cancer Sci. 94 (2003) 200—204.
[24] C. Dumontet, M.A. Jordan, Nat. Rev. Drug Discov. 9 (2010) 790—803.
[25] J.-H. Park, G.v. Maltzahn, L. Zhang, M.P. Schwartz, E. Ruoslahti, S.N. Bhatia, M.J. Sailor, Adv. Mater. 20 (2008) 1630—1635.
[26] J.-H. Park, G. von Maltzahn, L. Zhang, A.M. Derfus, D. Simberg, T.J. Harris, E. Ruoslahti, S.N. Bhatia, M.J. Sailor, Small 5 (2009) 694—700.
[27] Y. Ren, H.W. Cheung, G. von Maltzhan, A. Agrawal, G.S. Cowley, B.A. Weir, J.S. Boehm, P. Tamayo, A.M. Karst, J.F. Liu, M.S. Hirsch, J.P. Mesirov, R. Drapkin, D.E. Root, J. Lo, V. Fogal, E. Ruoslahti, W.C. Hahn, S.N. Bhatia, Sci. Transl. Med. 4 (2012) 147ra112.
[28] L. Roth, L. Agemy, V.R. Kotamraju, G. Braun, T. Teesalu, K.N. Sugahara, J. Hamzah, E. Ruoslahti, Oncogene 31 (2012) 3754—3763.
[29] G.M. Tozer, V.E. Prise, J. Wilson, M. Cemazar, S. Shan, M.W. Dewhirst, P.R. Barber, B. Vojnovic, D.J. Chaplin, Cancer Res. 61 (2001) 6413—6422.
[30] M.E. Åkerman, W.C.W. Chan, P. Laakkonen, S.N. Bhatia, E. Ruoslahti, Proc. Natl. Acad. Sci. USA 99 (2002) 12617—12621.
[31] P.P. Karmali, V.R. Kotamraju, M. Kastantin, M. Black, D. Missirlis, M. Tirrell, E. Ruoslahti, Nanomed.: Nanotechnol. Biol. Med. 5 (2009) 73—82.
[32] G. von Maltzahn, Y. Ren, J.-H. Park, D.-H. Min, V.R. Kotamraju, J. Jayakumar, V. Fogal, M.J. Sailor, E. Ruoslahti, S.N. Bhatia, Bioconjugate Chem. 19 (2008) 1570—1578.
[33] F. Yuan, M. Dellian, D. Fukumura, M. Leunig, D.A. Berk, V.P. Torchilin, R.K. Jain, Cancer Res. 55 (1995) 3752—3756.
[34] Z. Cheng, A. Al Zaki, J.Z. Hui, V.R. Muzykantov, A. Tsourkas, Science 338 (2012) 903—910.
[35] R.K. Jain, T. Stylianopoulos, Nature reviews, Clin. Oncol. 7 (2010) 653—664.
[36] B.C. Wilson, S.L. Jacques, IEEE J. Quantum Electron. 26 (1990) 2186—2199.
[37] Y. Nihei, Y. Suga, Y. Morinaga, K. Ohishi, A. Okano, K. Ohsumi, T. Hatanaka, R. Nakagawa, T. Tsuji, Y. Akiyama, S. Saito, K. Hori, Y. Sato, T. Tsuruo, Cancer Sci. 90 (1999) 1016—1025.
[38] M.E. Davis, J.E. Zuckerman, C.H. Choi, D. Seligson, A. Tolcher, C.A. Alabi, Y. Yen, J.D. Heidel, A. Ribas, Nature 464 (2010) 1067—1070.

[39] S. Sengupta, D. Eavarone, I. Capila, G. Zhao, N. Watson, T. Kiziltepe, R. Sasisekharan, Nature 436 (2005) 568—572.
[40] M. Martinelli, K. Bonezzi, E. Riccardi, E. Kuhn, R. Frapolli, M. Zucchetti, A.J. Ryan, G. Taraboletti, R. Giavazzi, Br. J. Cancer 97 (2007) 888—894.
[41] E.S. Wang, R. Pili, M. Seshadri, J. Clin. Oncol. 30 (2012) 760—761.
[42] D.A. Tice, W. Szeto, I. Soloviev, B. Rubinfeld, S.E. Fong, D.L. Dugger, J. Winer, P.M. Williams, D. Wieand, V. Smith, R.H. Schwall, D. Pennica, P. Polakis, J. Biol. Chem. 277 (2002) 14329—14335.
[43] M.J. Hope, M.B. Bally, G. Webb, P.R. Cullis, Biochim. Biophys. Acta 812 (1985) 55—65.
[44] L.D. Mayer, M.B. Bally, M.J. Hope, P.R. Cullis, Biochim. Biophys. Acta 816 (1985) 294—302.
[45] D.M. Euhus, C. Hudd, M.C. Laregina, F.E. Johnson, J. Surg. Oncol. 31 (1986) 229—234.
[46] M. Schwartz, Cancer 14 (1961) 1272—1294.

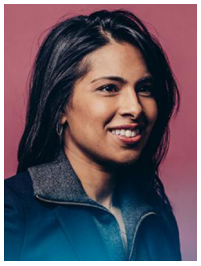

Dr. Sangeeta Bhatia is the John J. and Dorothy Wilson Professor of EECS and Institute for Medical Engineering and Science at MIT and an HHMI Investigator. Her lab focuses at the intersection of engineering, medicine, and biology to develop platforms that interface cells with synthetic systems for use in tissue regeneration, stem cell differentiation, medical diagnostics, and drug delivery. Dr. Bhatia's findings have produced human microlivers which model human drug metabolism, liver disease, and interaction with pathogens. Her group also develops communicating nanomaterials to interrogate and treat cancer. She has appointments at Brigham & Women's Hospital, Broad Institute, Harvard Stem Cell Institute, and MIT's Koch Institute and Ludwig Center. Dr. Bhatia received her B.S. from Brown University, M.S. and Ph.D. from MIT, M.D. from Harvard and completed graduate and post-doctoral training at MGH. Prior to MIT, she was tenured faculty at UCSD, and worked in industry at Pfizer, and others.

Kevin Lin is a graduate student in the Department of Chemical Engineering at MIT. His research focuses on the development of interactive nanosystems for the diagnosis and treatment of diseases including cancer and thrombosis. He received a B.S.E. degree in Chemical Engineering from the University of Michigan, Ann Arbor.

Ester Kwon is a postdoctoral researcher in the Division of Health Sciences and Technology at the Massachusetts Institute of Technology. She received her Ph.D. from the University of Washington in 2010 with Professor Suzie Pun developing peptide-modified nucleic acid delivery vehicles. Her current research interests are engineering peptide-decorated nanoparticles for applications in cancer and the central nervous system.

Justin Lo is an MD—PhD candidate at Harvard Medical School and MIT in the Division of Health Sciences and Technology. He received his B.S. in Biological Engineering from MIT. His present research focuses on designing targeted nanoparticles for therapeutic nucleic acid delivery to various types of cancer.

Supporting Information

Drug-Induced amplification of nanoparticle targeting to tumors

Kevin Y. Lin, Ester J. Kwon, Justin H. Lo, and Sangeeta N. Bhatia*

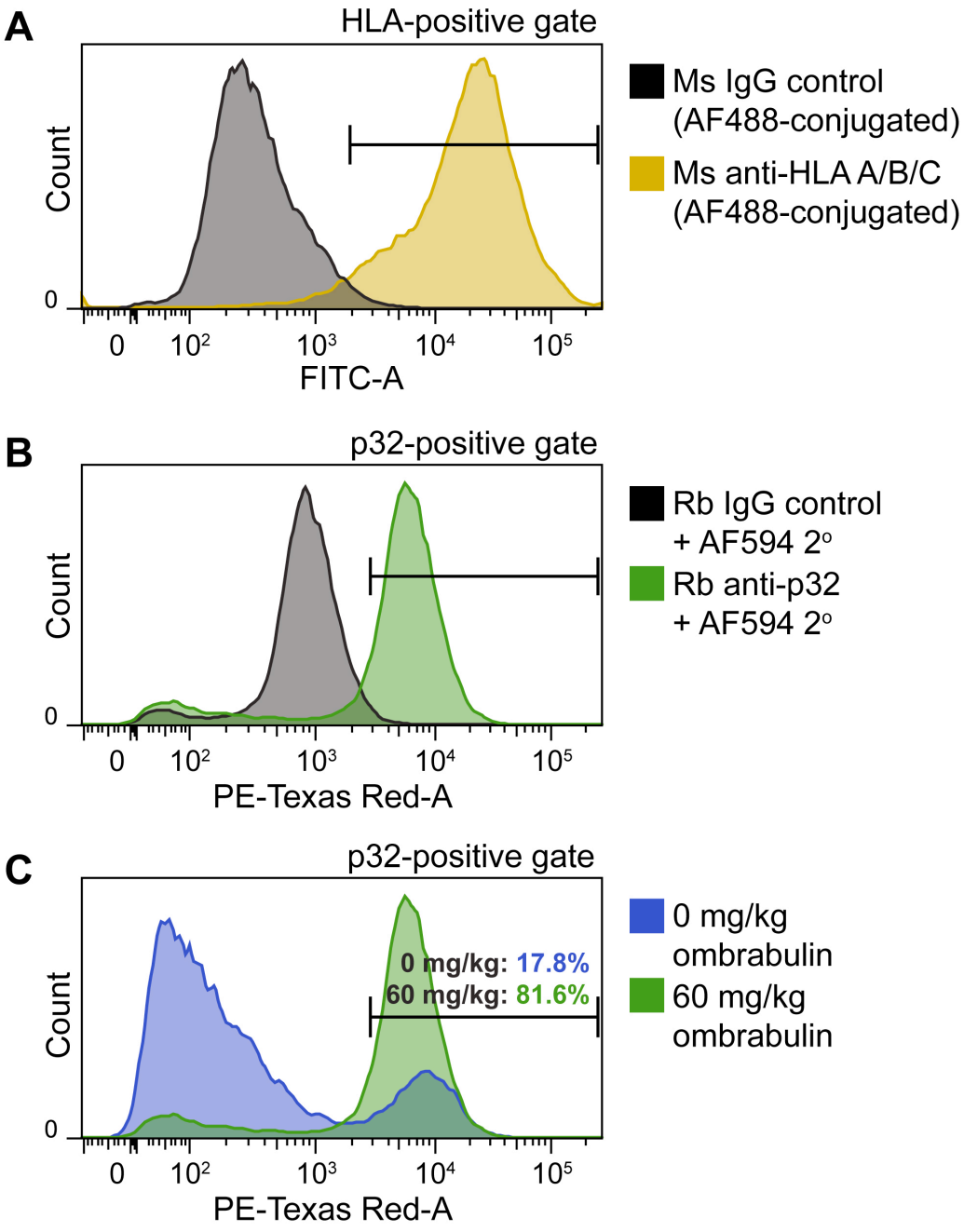

Figure S1. Flow cytommetry analysis of p32 expression on cells *ex vivo*. (A) Representative histograms of untreated MDA-MB-435 xenograft cells stained with AF488-conjugated mouse IgG control or AF488-conjugated mouse anti-HLA A/B/C, used to exclude non-xenograft cells from final analysis. (B) Representative histograms of *ex vivo* MDA-MB-435 cells 24-hours post treatment with ombrabulin (60 mg/kg), stained with either rabbit IgG control or rabbit anti-p32 antibody to establish the threshold for positive p32 staining. (C) Flow cytometry histogram of ex vivo MDA-MB-435 cells stained for p32 following treatment without (0 mg/kg) or with ombrabulin (60 mg/kg).

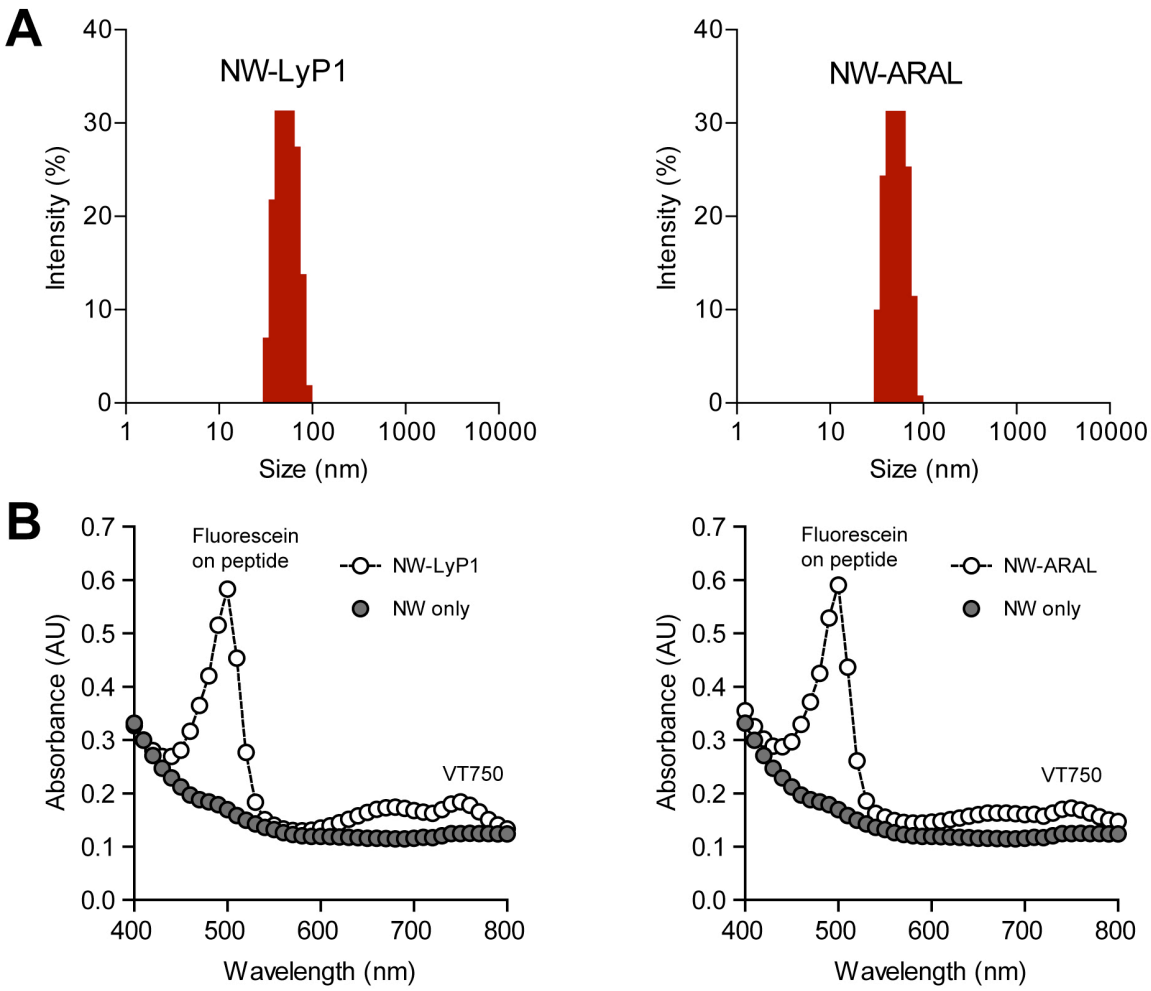

Figure S2. *In vitro* characterization of NWs. (A) Size distribution of iron oxide NWs as determined by dynamic light scattering. (B) Absorbance spectra of NWs conjugated with fluorescein-labeled peptides (~500 nm) and VT750 (~750 nm) and free NWs (grey).

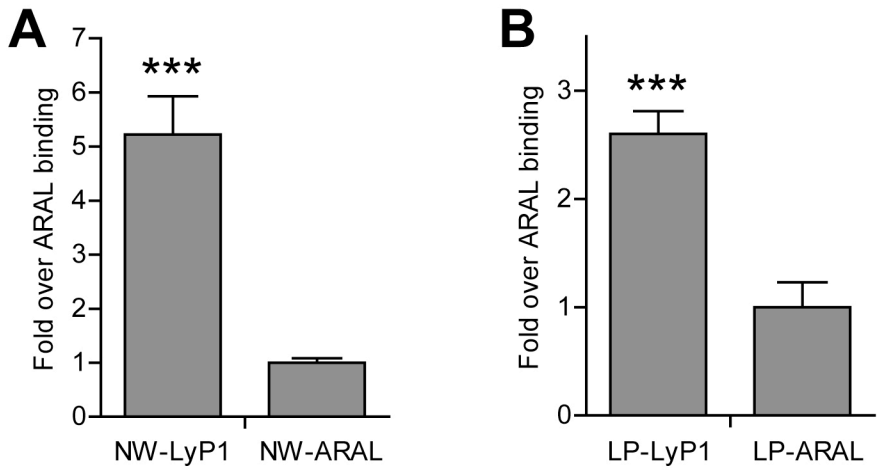

Figure S3. *In vitro* binding of NWs and LPs to recombinant p32. (A) Quantification of NW binding to p32 (*** $P < 0.005$, Student's *t*-test; n = 3, s.d.). (B) Quantification of LP binding to p32 (*** $P < 0.005$, Student's *t*-test; n = 3, s.d.).

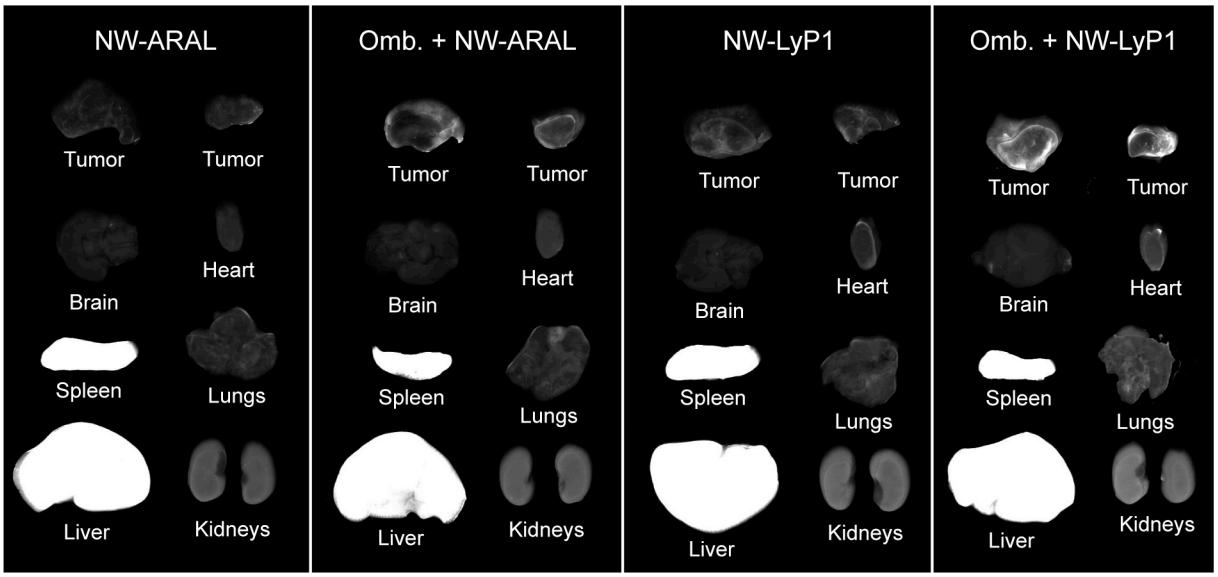

Figure S4. ***In vivo*** **biodistribution of NWs.** Near-infrared fluorescent scans of NW distribution in organs without (0 mg/kg) or with (60 mg/kg) ombrabulin (Omb.). Organs were excised and imaged at 24 hrs post-NW injection.

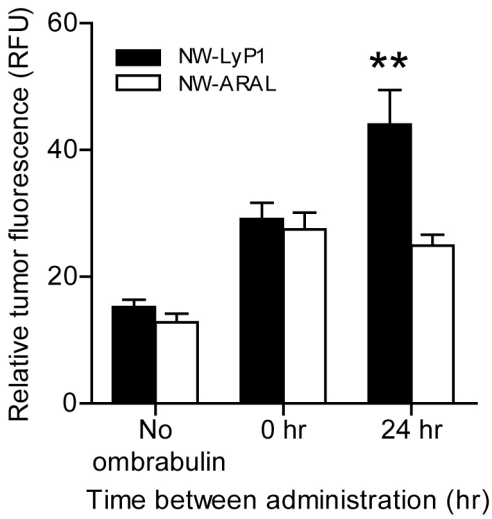

Figure S5. Effect of administration schedule on NW homing. Quantification of NW homing to tumors as a function of different times between ombrabulin (60 mg/kg) and NW administration (** $P < 0.01$, Student's *t*-test; n = 3–4 mice, s.e.).

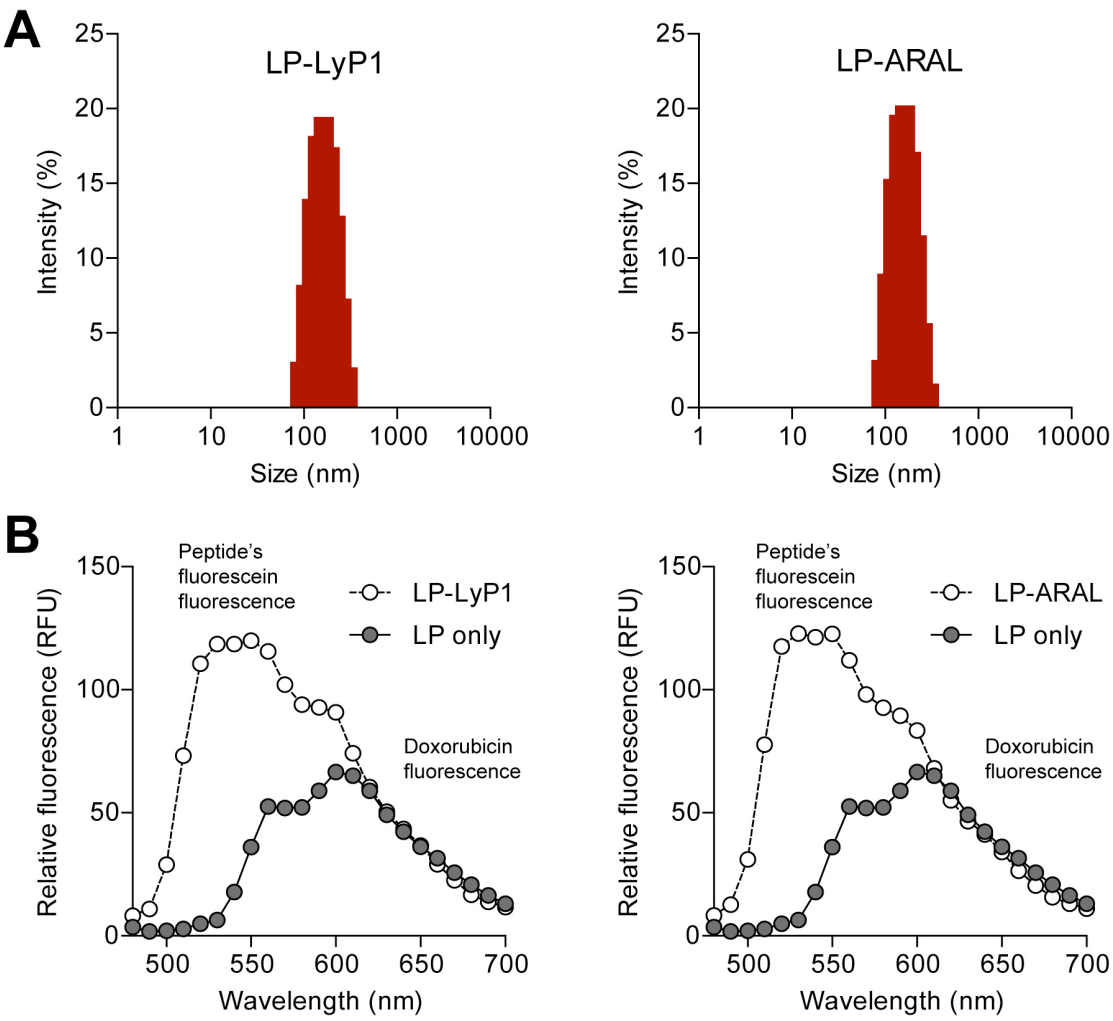

Figure S6. *In vitro* characterization of LPs. (A) Size distribution of doxorubicin-loaded LPs as determined by dynamic light scattering. (B) Fluorescence spectra of LPs conjugated with fluorescein-labeled peptides (excitation: 444 nm, emission: 480–700 nm, cutoff: 475 nm) and untargeted LPs (grey).

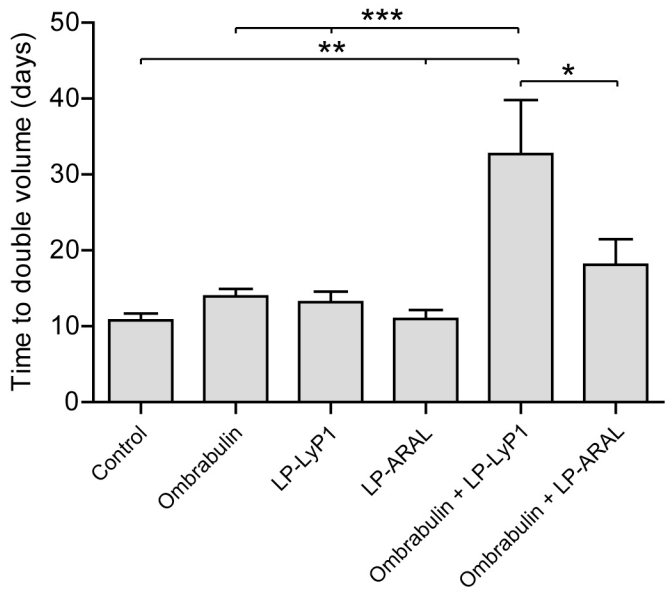

Table 1. Coefficient of determination

Treatment	**Average R^2**
Control	0.89
Ombrabulin	0.92
LP-LyP1	0.87
LP-ARAL	0.84
Ombrabulin + LP-LyP1	0.89
Ombrabulin + LP-ARAL	0.90

Figure S7. Tumor doubling time during therapeutic efficacy study. Calculated time to the doubling of tumor volume during the course of the therapeutic study (* $P < 0.05$, ** $P < 0.01$, *** $P < 0.005$, one-way ANOVA with Tukey post test; n = 7 mice, s.e.). Doubling time calculated by fitting tumor volumes to exponential growth curves. Table 1 shows the average coefficient of determination (R^2) of the curve fittings for each treatment group.